Photoluminescence of lithium thiogallate LiGaS$_2$

Alexander P. Yelisseyev,[1,]* Marina K. Starikova,[2] Valery V. Korolev,[3] Ludmila I. Isaenko,[1]
and Sergey I. Lobanov[1]

[1]*Institute of Geology & Mineralogy, Russian Academy of Sciences, Siberian Branch, 3 Academy Koptyug Avenue,
Novosibirsk 630090, Russia*
[2]*Novosibirsk State Technical University, 20 Karl Marx Avenue, Novosibirsk 630092 Russia*
[3]*Institute of Chemical Kinetics and Combustion, Russian Academy of Sciences, Siberian Branch, 3 Institutskaya Street,
Novosibirsk 630090, Russia*
Corresponding author: eliseev.ap@mail.ru

Annealing in appropriate atmosphere affects considerably transparency and photoluminescence (PL) of lithium thiogallate LiGaS$_2$ (LGS). Intense absorption at 8.0 µm after annealing in vapors of Ga$_2$S$_3$ or S is related to S–S vibrations. Annealing in vacuum produces intense blue PL in a 2.74 band, which transforms further to a 2.98 eV band: both emissions are excited in the same 3.4 eV band and are associated with two types of crystallographically nonequivalent anion vacancies (*F*-centers). The 2.98 eV emission of a more stable *F*-center decays exponentially with decay times $\tau = 19$ µs and 218 ns at 80 and 300 K, respectively, and quenches to 650 K. PL in a 2.0 eV band, excited near the fundamental absorption edge, with a large Stokes shift and fast temperature quenching is related to recombination of the self-trapped excitons. LGS with *F*-centers can be used as a light-emitting medium in different laser and optoelectronic devices.   © 2012 Optical Society of America
    OCIS codes: 300.6250, 300.6280, 140.3380.

1. INTRODUCTION

Optical parametric oscillation (OPO) is today one of the most widespread ways to produce tunable coherent radiation. The main part of OPO is a nonlinear crystal. The most widely used nonlinear crystals for the mid-IR are silver thiogallates and selenogallates (AgGaS$_2$ and AgGaSe$_2$), zinc germanium phosphide ZnGeP$_2$, etc. [1]. Recently, ternary chalcogenides related to the LiB$^{\mathrm{III}}$C$_2^{\mathrm{VI}}$ family where $B =$ In, Ga and C = S, Se, Te are also considered promising nonlinear crystals [2,3]. The advantages of these crystals are their relatively high thermal conductivity, large bandgap, and, as a result, a low two-photon absorption and a weak mismatch between the group velocities [4]. The LiGaS$_2$ (LGS) crystals have the largest bandgap and maximal threshold of optical damage among LiB$^{\mathrm{III}}$C$_2^{\mathrm{VI}}$ compounds [4]. Because of the high volatility of chalcogen and large chemical activity of Li, it is difficult enough to grow LGS crystals of stoichiometric composition. The deviations from stoichiometry lead to inclusions of foreign phases and increased content of native point defects, which in turn lower crystal transparency and affect negatively the OPO output parameters. When investigating how LGS annealing affects its optical properties, we found an intense photoluminescence (PL) in the shortwave (violet to blue) region, which appears after annealing in vacuum and disappears after annealing in the sulfur-containing atmosphere. This PL was associated with anion vacancies (*F*-centers), and in the present paper we studied its optical properties in detail. We revealed two types of *F*-centers corresponding to two crystallographically nonequivalent S sites in LGS, investigated PL kinetics and thermal properties. Low-temperature pink PL present in all LGS crystals is associated with the recombination of self-trapped excitons (STEs).

2. EXPERIMENTAL TECHNIQUE

A. Crystal Growth

LGS single crystals were grown using the Bridgman–Stokbarger technique in a two-zone vertical furnace. Its upper and lower parts were separated with a diaphragm from a poorly thermoconductive material. The temperature of melted zone was kept at the level of 1150 °C with accuracy of ± 0.1 °C, which is ~100 °C higher than the LGS melting temperature. Axial temperature gradient was ~2 °C.mm^{-1}. The rate of ampule dropping varied in the range of 2 to 10 mm/day. We used Ga and S of 99.999% purity and Li 99.9% as starting chemicals for crystal growth. The charge was placed into a glass graphite crucible, which in turn was sealed into a silica ampule. Such construction allowed us to weaken a chemical interaction between Li and the container (silica) walls. Grown LGS single crystals were ~20 mm in diameter and up to 50 mm long. We cut ~2 mm thick plates with 0.5 cm^2 aperture; their edges were parallel to crystallographic axes. These LGS plates were annealed at $T = 950$ °C in static vacuum or in the presence of solid Li$_2$S, Ga$_2$S$_2$, or S in order to lower the light scattering and improve the transparency. The annealing experiments on LiInS$_2$, combined with composition testing using the technique of differential dissolving [5], showed changes up to 2 wt. % for different components after annealing. The LGS plates were polished after annealing before the spectroscopic measurements. To analyze the shape of fundamental absorption edge, thin ~60 µm thick polished plates were prepared.

B. Crystal Structure

Compounds LiInS$_2$ (LIS), LiInSe$_2$ (LISe), LiGaS$_2$, and LiGaSe$_2$ (LGSe), related to the LiB$^{\mathrm{III}}$C$_2^{\mathrm{VI}}$ family with a tetrahedral atom

coordination, crystallize in orthorhombic structure β-FeNaO$_2$ with space group Pna2$_1$ (point group mm2). Compounds A^{I}B^{III}C$_2^{VI}$, where A^I is an alkali metal, B^{III} are Ga, In, and C^{IV}, a chalcogen, is S, Se, or Te, are characterized as structures with mixed covalent-ionic types of bonding [6]. Here the A^I–C^{VI} bonds are mainly ionic, whereas the B^{III}–C^{IV} bonds are mainly covalent. The lithium has a very low electronegativity (compared to sulfur's), and thus strong bond ionicity; as a result, chemical bonds are the strongest, and bandgap is the largest. The structure of LGS is formed by Li–S$_4$ and Ga–S$_4$ tetrahedrons, and the S^{2-} ions are arranged in hexagonal packing with tetragonal and octahedral cavities (tetrapores and octapores). Only half of the tetrapores are occupied by Li and Ga, while all octapores are empty. LGS structure is shown in Fig. 1. The β-NaFeO$_2$ structure is less dense than the chalcopyrite structures of AgGaS$_2$ and AgGaSe$_2$ due to the presence of these empty cavities in the unit cell volume. There are two anion-centered tetrahedrons Li$_2$Ga$_2$: they are titled S_1 and S_2 in [6] (Fig. 2). Both tetrahedrons are distorted in different ways, and, as a result, the lengths of Li–S and Ga–S bonds as well as the angles between them are all different (Table 1). The difference between the longest and the shortest Li–S bonds is 0.0301 nm, whereas for Ga–S bonds this value is 0.0084 nm (Table 1). Larger lengths of bonds are typical of S_1, whereas for S_2 the lengths are shorter (Table 2). As follows from Table 1, in the A^{I}B^{III}C$_2^{VI}$ family these differences are maximal in LGS. This implies that the bond energies for S are considerably different in Li$_2$Ga$_2$ tetrahedrons with S_1 and S_2.
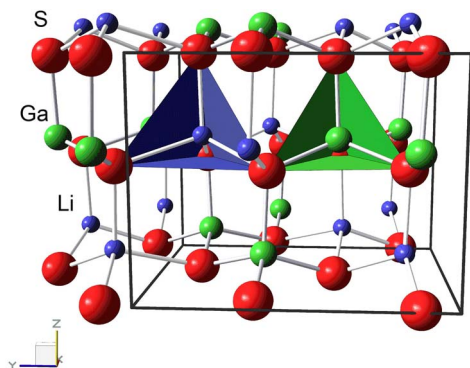

Fig. 1.   (Color online) Structure of LGS crystal of space group Pna21 with tetrahedrons: Li–S_4 (left) and Ga–S_4 (right). Blue, green, and red balls correspond to Li, Ga, and S atoms, respectively.
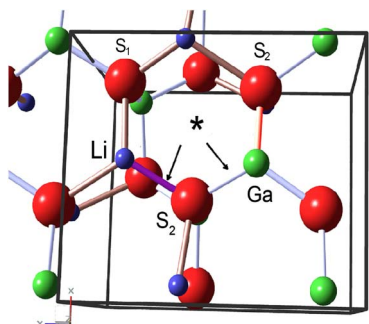

Fig. 2.   (Color online) Fragment of LiGaS$_2$ structure with two sulfur sites: S_1 and S_2. The shortest bonds are marked by an asterisk.

Table 1.   Distortions in LiC$_4$, BC$_4$ Tetrahedrons in LiBC$_2$ Crystals

Crystal	LGS	LGSe	LIS	LISe
R(Li^{+1}), nm	0.045	0.047	0.045	0.047
R(B^{+1}), nm	0.042	0.044	0.045	0.047
ΔLi–Hal, nm	0.0301		0.0142	0.0181
ΔB–Hal, nm	0.0084		0.0017	0.0009

Table 2.   Bond Lengths in Tetrahedrons Li$_2$Ga$_2$, Containing S_1 and S_2

Sulfur Site	Bonds	BondLength/Distance, nm ($\pm$0.0002 nm)
S_1	Li–S	0.2410
	Li–S	0.2590
	Ga–S	0.2271
	Ga–S	0.2261
S_2	Li–S	0.2260
	Li–S	0.2269
	Ga–S	0.2252
	Ga–S	0.2364

C. Optical Spectroscopy and Irradiation

Transmission spectra were recorded using a UV-2501PC Shimadzu spectrometer in the UV to near IR, whereas in the mid-IR we used a Fourier transform spectrometer Infralum 801. The PL spectra were measured using an SDL1 luminescence spectrometer with excitation from the 1 kW Xe lamp through the MDR2 monochromator. The photoluminescence excitation (PLE) spectra were corrected to a constant number of incident photons using Na salicylate and Rhodamine 640. Maximal possible transmission T_∞ and LGS absorption were calculated using dispersion characteristics $n = f(\lambda)$ for LGS from [7] and the well-known formulas for single reflection,

$$R = \frac{(n-1)^2}{(n-1)^2}, \tag{1}$$

and transmission at multiple reflection [8],

$$T_\infty = \frac{1 - R^2}{(1 - R)^2}. \tag{2}$$

PL kinetics was measured at excitation from the XeCl excimer laser ($\lambda = 308$ nm, $\tau = 20$ ns) and the third harmonic of the Nd:YAG laser (355 nm, ns) with an Edinburgh Instruments F900 spectrometer. The PL quantum yield η was measured relative to the freshly prepared sodium salicylate powder, which has a reported quantum efficiency of $\eta = 0.99$ when excited at 253.7 nm [9]. The ionizing irradiation with fast electrons was carried out on the linear electron accelerator at the Institute of Chemical Kinetics and Combustion, Novosibirsk. The electron energy was 3.5 MeV, and the dose was $\sim 10^{17}$ cm^{-2}. Crystals were cooled by flowing cold water during irradiation. Raman spectra were measured using a Ranishaw Ramascope Raman spectrometer.

3. RESULTS AND DISCUSSION

A. Raman Spectrum

The Raman spectrum, recorded for LGS at $T = 300$ K, is given in Fig. 3. The group-theory analysis shows that, at the zone center for the β-NaFeO$_2$ structure, the 48 normal phonon modes are distributed among various irreducible representations of the C_{2v}^9 factor group as follows: $\Gamma^{\text{vib}} = 12A_1 + 12A_2 + 12B_1 + 12B_2$. As in the case of LiInS$_2$ [10], the three acoustic phonon modes have A_1, B_1, and B_2 symmetries; the 45 remaining (optical) modes are Raman active. Owing to the respective mass of the atoms, high- (low-) frequency modes obviously imply the movements of Li–S (Ga–S) bonds. Phonons of medium frequency (250–350 cm^{-1}), visible in both IR reflectivity and Raman scattering, are attributed to Ga–S bonds. The phonons of highest frequency (above 350 cm^{-1}) that give rise to strong IR bands but are not observable in Raman spectra are due to weaker Li–S bonds. Larger energies for Me$^{\text{I}}$–C$^{\text{VI}}$ vibrations in LiGaS$_2$ in comparison with AgGaS$_2$ with chalcopyrite structure favor heat dissipation; hence, a higher thermal conductivity is expected. The thermal conductivity of LiGaS$_2$ is not known to date but is expected to be close to that of LiInS$_2$. The thermal conductivity of LiInS$_2$ varies from 6.0 to 7.6 Wm^{-1}K^{-1} for different directions [10] and is ~5 times higher than that of AgGaS$_2$.

B. Transmission/Absorption Spectra and Defect Concentration

The transmission spectra for LGS crystals annealed in different environments are shown in Fig. 4. At room temperature, all LGS samples are transparent in the 0.32–11.6 μm range above the transmission level of 10%, which corresponds approximately to the absorption level of 5 cm^{-1}. The shortwave limit in the UV is determined by the fundamental absorption edge of LGS, whereas multiphonon absorption is responsible for the longwave limit: two-phonon and three-phonon absorption limits setting on from about 10 and 7 μm, respectively. To determine bandgap precisely, we recorded transmission spectra of the 60 μm thick LGS plate at 80 and 300 K. The analysis of the shape of the fundamental absorption edge showed that linear approximation is possible for the $(\alpha h\nu)^2$ versus $h\nu$ curves. This implies the case of direct, allowed band-to-band electronic transitions (Fig. 5) [8]. This direct-allowed transition feature is also confirmed by the first-principles calculations for LGS in [11]. Extrapolation of linear part
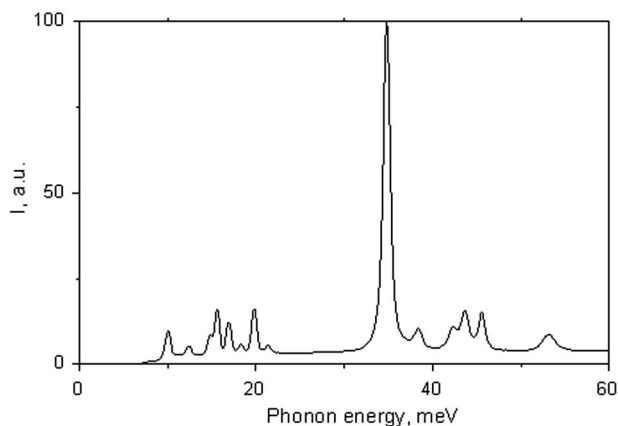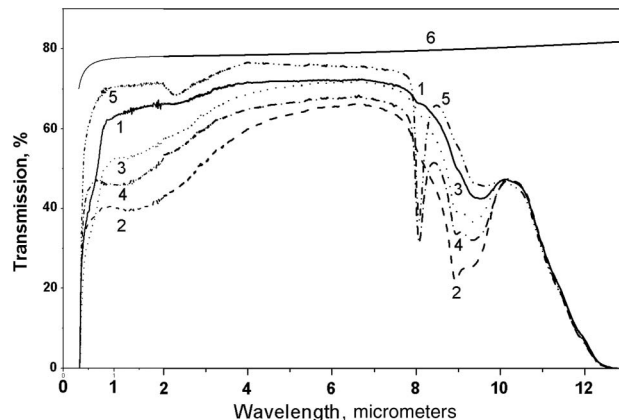

Fig. 4. Transmission spectra of the 2 mm thick LGS samples recorded at room temperature after annealing in different environments: as-grown LGS (Curve 1), in vacuum (Curve 2), and in the presence of vapors of Li$_2$S (Curve 3), Ga$_2$S$_3$ (Curve 4), and sulfur (Curve 5). Curve 6 shows the maximum possible transmission of LGS calculated supposing zero absorption and multiple reflections and using $n = f(\lambda)$ from the Sellmeier equation in [8].

to $\alpha(h\nu) = 0$ gives the E_g values 3.93 ± 0.01 and 4.03 ± 0.01 eV at 300 and 80 K, respectively. As temperature increases from 80 to 300 K, the bandgap E_g shifts by 0.1 eV to lower energies: such a shift is rather typical of wide-gap dielectrics [12]. It is necessary to remind that the bandgap of LGS was estimated as 4.15 eV at room temperature in the previous papers [7,13] where the measurements were carried out on thick samples ($L = 2$ mm), and there was a strong (~20 cm^{-1}) absorption band centered at ~330 nm near the fundamental absorption edge. In this work a considerably thinner plate ($L = 60$ μm) is used, which allowed us to measure absorption coefficients up to 10^3 cm^{-1}, and there were no strong bands in LGS samples under investigation. The intensity of absorption bands near the fundamental absorption edge did not exceed 3 cm^{-1} value (Fig. 6). Therefore, the current estimation of the E_g value is supposed to be more accurate. These E_g values are maximal among the crystals of the Li$^{\text{I}}$B$^{\text{III}}$C$_2^{\text{VI}}$ family. For other crystals, the E_g values are 3.57 eV for LiInS$_2$ [10], 2.9 eV (LiInSe$_2$) [14], 3.34 eV (LiGaSe$_2$) [7], and 2.3 eV (LiGaTe$_2$) [7] at 300 K.

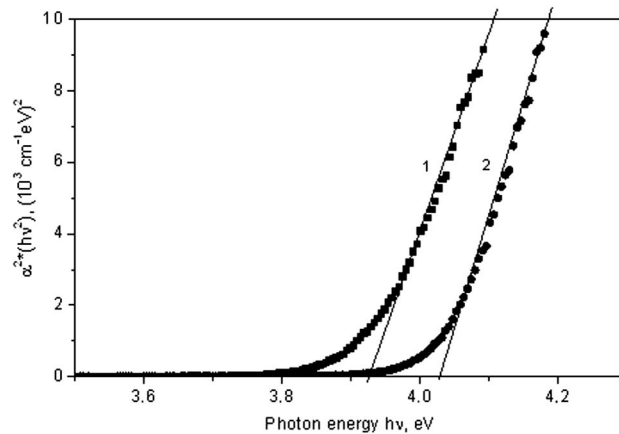Fig. 3. Unpolarized Raman spectra for LGS at $T = 300$ K.

Fig. 5. Fundamental absorption edge for a 60 μm thick plate cut from "as-grown" LGS sample, at 300 K (Curve 1) and 80 K (Curve 2). Bandgap values E_g are 3.93 ± 0.01 and 4.03 ± 1 eV, respectively.
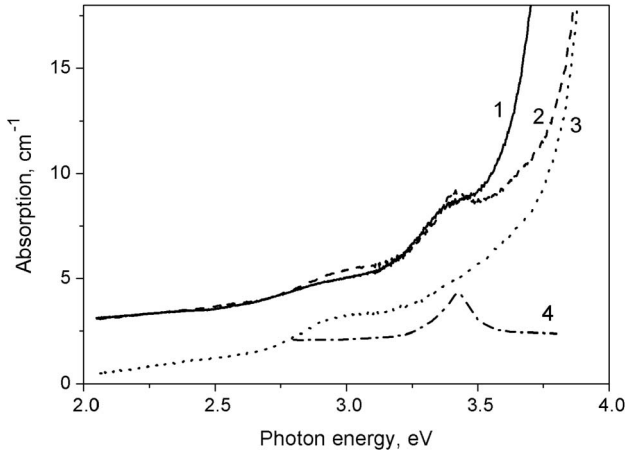
Fig. 6.   Absorption spectra at 300 K (Curve 1) and 80 K (Curves 2 and 3) for 2 mm thick plates cut from as-grown LGS (Curve 1) and from LGS annealed in vacuum (Curve 2) and in *S* vapor (Curve 3). Curve 4 is differential spectrum (Curves 2 and 3).

Most of the LGS transmission spectra in Fig. 4 demonstrate considerable optical losses in the 0.3–4 eV (0.3–5 μm) spectral region combined with a set of broad absorption bands near both shortwave and longwave transparency edges. The intensity of losses at $\lambda < 5$ μm correlates with the light scattering revealed at the visual examination of the polished LGS crystals. The intensity of these losses falls steadily as the wavelength increases, and at least a part of these losses is due to the Rayleigh light scattering on the submicrometer inclusions of foreign phases. The cross section of nonresonant Rayleigh scattering is $\sigma \sim \lambda^{-4} r^6 (\varepsilon - \varepsilon_0)$, where r is the size of scattering particles (inclusions in our case) with $r \ll \lambda$ and ε and ε_0 are the dielectric permittivity of scattering substance and the surrounding medium (crystal). It follows from this formula that the scattering is maximal at short wavelengths and decreases to the mid-IR. Such optical losses are typically strong in the as-grown boules of ternary chalcogenides, including AgGaS$_2$, AgGaSe$_2$, and LiInS$_2$; their as-grown boules are milky [7,13,15]. Another possible reason of optical losses in the LGS transparency range may be the optical absorption of broken bonds in dislocations: the latter are known to produce a continuous set of levels in the forbidden zone [16]. A widespread technique to improve the transparency of an as-grown chalcogenide crystal is to anneal it in an appropriate atmosphere. In this work, we annealed as-grown LGS crystals in vacuum and in S, Li$_2$S, and Ga$_2$S$_3$ environments: in this way we tried to affect the Li, Ga, and S contents in LGS and their spectroscopic properties.

We established that only annealing in sulfur vapor improves the overall transparency in the as-grown LGS despite a strong optical absorption band at 8.0 μm and a considerably weaker 2.5 μm band (Fig. 4). The other treatments increase the light scattering [13] and produce also a broadband absorption at 9.3 μm with a narrower component at 8.9 μm. The 8.9/9.3 μm components are related to the Ga–O vibrations [17], revealing the trace of oxygen contamination in the LGS crystal. Strong absorption at 8.0 μm, appearing after annealing in vapors of Ga$_2$S$_3$ and sulfur, is associated with the S–S vibration, which was also observed in the chalcogenide glasses [17]. We suggest that such annealing does compensate the existing deficit in S in the as-grown LGS and even creates

the surplus. Thus, the improvement in the transparency after annealing in the S vapor implies that indeed there was a deficit in sulfur in as-grown LGS. Furthermore, occurrence of S–S vibrations indicates that some sulfur atoms are in close adjacent positions. The absence of such S–S pairs in the perfect LGS structure suggests that some S atoms occupy the interstitial positions or cation (Li or Ga) sites. Taking into account that the 8.0 μm absorption band appears only after annealing in Ga$_2$S$_3$ (not in Li$_2$S), one may conclude that S is more likely to occupy the Li site (not Ga site). This result is consistent with the fact that the size of Li (0.045 nm) is somewhat larger than that of Ga (0.042 nm), so the S anions are favored to replace the Li sites. Another explanation of this fact is a much higher Gibbs energy for one S ion in the case of Li$_2$S in comparison with Ga$_2$S$_3$, −520 kJ.mol^{-1} and −226 kJ.mol^{-1} at 600 °C, respectively [18]. Consequently, Li$_2$S is much more stable than Ga$_2$S$_3$ and so reacts much less. It could be a reason why Li$_2$S is less reactive during annealing.

In the shortwave region near the fundamental absorption edge, we observed a weak band at 2.95 eV in all LGS crystals and an additional band at 3.31 eV in LGS crystals annealed in vacuum. The latter is better pronounced in the differential spectrum (Fig. 6, Curve 4). This spectrum was obtained when subtracting Curve 3, without 3.31 eV band, from Curve 2 with this band. On the other hand, the 3.31 eV band disappears after annealing in the presence of S-containing solids (Li$_2$S, Ga$_2$S$_3$, or S). It is possible to associate the 3.31 eV band with an anion (sulfur) vacancy V_S. These defects appear when some of S atoms are removed (at annealing in vacuum) but they disappear when sulfur is added again at annealing in Li$_2$S, Ga$_2$S$_3$, or S and empty S sites are filled with S atoms again. These defects are known as F-centers in literature [19]. Anion vacancy has a deficit of electrons, and its charge state should be (2+). Normally such centers capture deficient electrons from some other defects, and vacancy becomes neutral (F^0 state). These centers were studied in detail for alkali haloids, oxides, fluorides, etc. [19]. It is noteworthy that the F-centers may become ionized at appropriate illumination passing to F^+ state [19].

The defect concentration N can be estimated from the absorption spectrum, using the well-known Smakula's formula [19]:

$$N(\text{cm}^{-3}) = 0.821 \times 10^{17} \frac{n}{(n^2 + 2)^2 f_{ij}} \int \alpha(E) \mathrm{d}E \qquad (3)$$

where n is the refractive index for LGS in the environment of the absorption bands, f_{ij} is the oscillator's strength, $\alpha(E)$ is the absorption coefficient (cm^{-1}), and E is the photon energy (electron volts). For the Gaussian case, which takes place in LGS, Eq. (3) transforms to

$$N(\text{cm}^{-3}) = 0.87 \times 10^{17} \frac{n}{(n^2 + 2)^2 f_{ij}} \times \alpha_{\max} \gamma, \qquad (4)$$

where $\alpha_{\max}$ is the maximum absorption and γ is the full width at half-maximum (FWHM) of the absorption band (electron volts).

Taking $n \sim 2.3$ at the photon energy of about 3 eV for LGS [7], the FWHM values 0.16 and 0.31 eV for absorption bands 3.4 and 2.95 eV, respectively, and $\alpha_{\max} = 2.0$ and 0.9 cm^{-1}, respectively, we obtain $N(3.4 \text{ eV}) = 1.2 \times 10^{15}/f$ and

$N(2.95 \text{ eV}) = 1.02 \times 10^{15}/f$ for defect concentrations. For the case of $f = 0.1$, which is the typical oscillator strength for F-centers in LiF and NaF [18], the defect concentrations N are about 10^{16} cm^{-3} for both 3.4 and 2.95 eV bands.

C. PL Spectra

Figure 7 shows the PL spectra recorded at 80 K at different excitations for the same LGS sample annealed in vacuum: spectra in Fig. 7a were recorded shortly (in several days) after annealing, whereas those in Fig. 7b were recorded in about six months after annealing. In both cases band-to-band excitation at 4.2 eV produces a pink PL in a broad band centered near 1.92 eV (650 nm), and FWHM = 0.5/0.6 eV. This PL was observed in LGS samples annealed in the presence of Li$_2$S, Ga$_2$S$_3$, and S. The PL intensity weakens an order as temperature grows from 80 to 300 K; complete quenching occurs at 400 K.

Considerably different situation takes place at excitation into the 3.4 eV related to the F-centers. An intense blue PL is typical of LGS annealed in vacuum, and some time later the PL color changes to violet, the intensity remaining high. Corresponding PL spectra are given in Figs. 7a and 7b. It is necessary to note that the structure of both PL spectra is somewhat similar: in both cases there are three broad bands. The bands' maxima are 2.74, 2.34, and 1.93 eV (452, 529, and 660 nm), and their FWHM values are 0.22, 0.26, and 0.42 eV for LGS shortly after annealing (Curve 2). The parameters are different in six months: the PL maxima become 2.98, 2.42, and 1.93 eV (415, 512, and 642 nm), and the FWHM values are 0.30, 0.38, and 0.5eV (Curve 4). High-energy components at 2.74 and 2.98 eV are the most intense in both cases. Thus, it seems that two high-energy components shift simultaneously to high energy as time passes, whereas the low-energy components remain the same.

Two high-energy components quench much slower as temperature grows in comparison with the third component (Fig. 8). Their intensity decreases only by ~50% as temperature grows from 80 to 300 K and the complete quenching occurs at 600 K, whereas the third low-energy component disappears already at 400 K. Changes in PL spectrum as temperature grows for case in Fig. 7b are shown in Fig. 8.

Fig. 8. PL spectra for V_{S2} at 3.35 eV excitation, recorded at 80, 150, 200, 330, 450, and 550 K (Curves 1, 2, 3, 4, 5, and 6, respectively), in six months after annealing LGS in vacuum. Detail with two low-energy peaks is shown in the inset.

D. PLE Spectra

The PLE spectra for the main PL bands in LGS are given in Fig. 9. Curve 1 is PLE for the pink PL in all LGS crystals. One can see that this emission is excited mainly in the 3.94 eV band, located near the fundamental absorption edge as well as at band-to-band transitions (arrow shows $E_g = 4.03$ eV) and behind the edge when only the near-surface layer is excited. Maximums near 5 eV correspond to features in the function of the density of states in valence and conduction bands. Pink PL is excited also but with a lower efficiency in the 2.9 and 3.4 eV bands.

Curve 2 in Fig. 9 shows PLE for both blue and violet PL types in LGS, annealed in vacuum, with dominating peaks 2.74 eV and 2.98 eV, respectively. Their PLE spectra are identical: at 80 K they consist of two close bands with maxima at 3.28 eV (377 nm) and 3.38 eV (366 nm), their FWHM values being 0.09 and 0.13 eV, respectively. This shows that the excited state of this defect is split ~0.1 eV. As temperature increases, the maxima of these components shift to low energies, bands are broadened, and the input of the low-energy component decreases. The Stokes shift is 2 eV for pink PL,
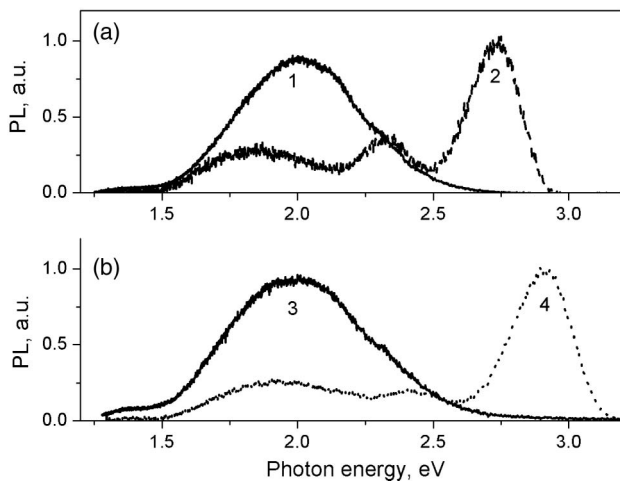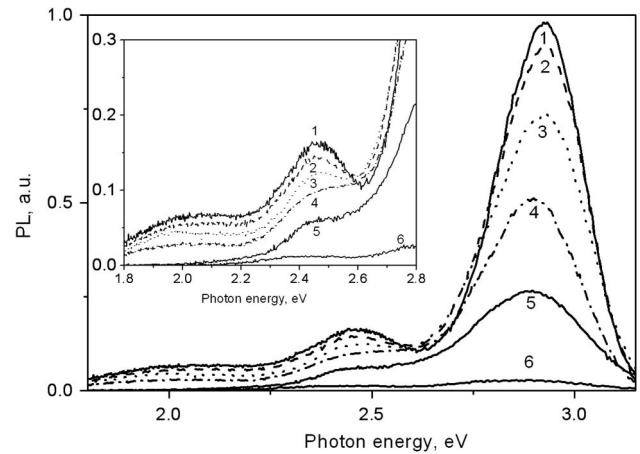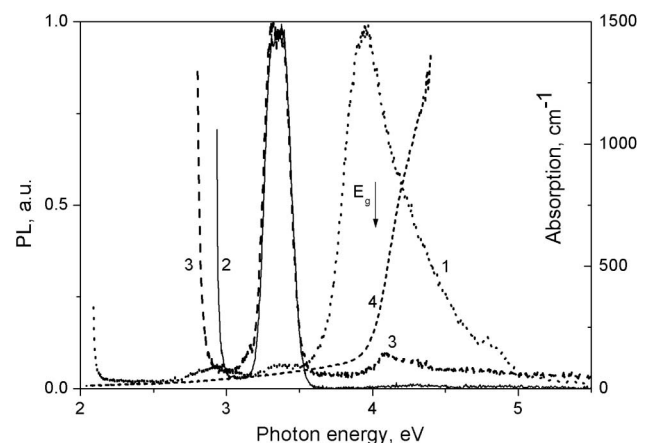

Fig. 7. PL spectra for LGS, measured a. shortly after annealing in vacuum and b. in six months at 4.2 eV excitation (Curves 1 and 3) and 3.35 eV excitation (Curves 2 and 4). $T = 80$ K.

Fig. 9. PLE spectra for PL bands at 1.92 eV (Curve 1), 2.92 (Curve 2), and 2.75 eV (Curve 3) at $T = 80$ K in LGS. Curve 4 is absorption spectrum for 60 μm thick LGS plate at 80 K . Arrow shows bandgap Eg = 4.03 eV at 80 K.
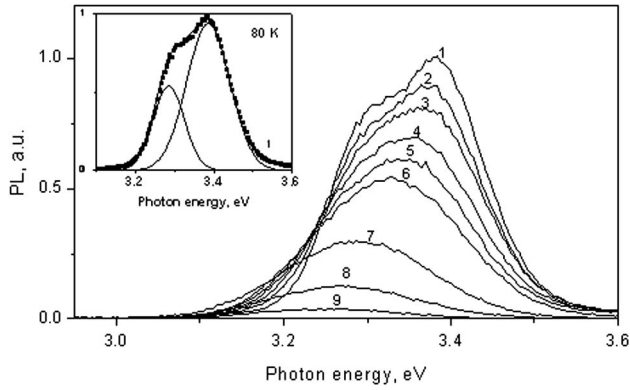
Fig. 10.   PLE spectra for PL band 2.98 eV (415 nm) in LGS, in six months after annealing in vacuum. Spectra were recorded at 80, 135, 175, 200, 240, 315, 490, 530, and 590 K (spectra 1, 2, 3, 4, 5, 6, 7, 8, and 9, respectively). (Inset) The experimental PLE spectrum for 2.98 eV PL at 80 K is shown by points, whereas the solid line spectra are a result of its decomposition into Gaussian components.

and it is much lower for the blue 2.74 eV ($\Delta = 0.64$ eV) and violet 2.98 eV ($\Delta = 0.40$ eV) bands.

The identity of absorption and PLE spectra for centers responsible for the blue 2.74 eV and violet 2.98 eV PL in LGS after annealing in vacuum, similarity of their PL spectra (doublets with dominating high-energy component) and of the PL temperature dependence (slow quenching to 600 K), similar formation conditions (appearing after annealing in vacuum and disappearance after annealing in the presence of S-containing solids), and at least their transformation into each other with the lapse of time allows us to conclude the following.

1. These two centers should be similar in structure.
2. Both centers are anion (sulfur) vacancies, *F*-centers.
3. Taking into account the presence of two crystographically nonequivalent positions for sulfur in LGS lattice (S_1 and

S_2, Fig. 2, Table 2) these two centers are suggested to be vacancies in these two S sites. The S_2 site has shorter and stronger bonds relative to the S_1 site and it must be more stable.

4. A transient center V_{S1} with the main 2.74 eV band in PL is formed more easily but it later transforms into another V_{S2} state characterized by the 2.986 eV PL. This $V_{S1} \rightarrow V_{S2}$ transformation can be a result of photoinduced transitions when stocking and their study is progress now.

The pink PL in the broad band near 2 eV, which is observed in all LGS crystals and depends slightly on the annealing conditions, excited mainly in the 3.94 eV band below the E_g with a large Stokes shift of 2 eV is likely related to the recombination of STEs [20].

E. PL Decay Kinetics

The kinetics of PL decay was measured only for the most stable V_{S2} component. We recorded a decay of violet emission at 2.88 eV (430 nm) and of pink emission at 2.25 eV (550 nm). To excite PL, we used an excimer laser operating at $h\nu = 3.99$ eV and the third harmonic of the Nd:YAG laser (3.49 eV). The results are given in Fig. 11 for 80 (Figs. 11a and 11c) and 300 K (Figs. 11b and 11d) (see below). As one can see from Figs. 11a and 11b, the violet PL decay is well approximated by exponents with decay time $\tau = 19.0 \pm 0.5$ μs at 80 K and $\tau = 218 \pm 2$ ns at 300 K. The decay time decreases 2 orders as temperature grows. The exponential PL decay indicates the intracenter recombination process in the *F*-center at both 80 and 300 K.

The excimer laser excites the pink broadband PL, the spectrum of which is shown by Curve 4 in Fig. 7. The PL kinetics is more complicated and becomes considerably faster as temperature increases from 80 to 300 K. The PL kinetics may be approximated by a sum of two exponents with decay times 1.5 and 7.5 μs at 80 K, and 58 and 300 ns at 300 K. One can see that decay time decreases ~20 times for both components as
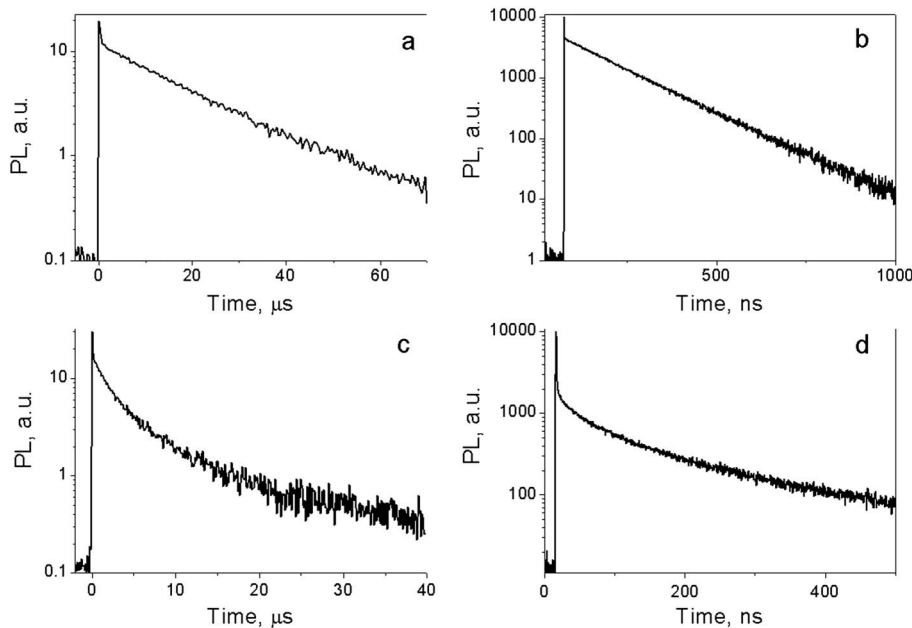

Fig. 11.   PL decay at 80 and 300 K (b, d) in LGS in six months after annealing in vacuum. PL was excited by the third harmonic of the Nd:YAG laser at 3.49 eV/355 nm (a, b) and by excimer laser at 3.99 eV/308 nm (c, d). PL was measured at 2.88 eV (a, b) and 2.25 eV (c, d). PL intensities are given in the logarithmic scale.

temperature grows from 80 to 300 K. Simultaneously, intensity of the pink PL decreases considerably.

F. Temperature Dependence of PL and PLE Intensities

The behavior of PL and PLE spectra related to the F-centers versus temperature is shown in Figs. 8 and 10, respectively. The following changes are observed as temperature grows: (i) the integral PL intensity decreases steadily; (ii) the peaks maxima shift to lower energies, and (iii) the band FWHM increases. The quantum efficiency η of violet PL of V_{S2}, estimated relative to freshly prepared sodium salicylate, was found to be close to 1 at 80 K. We took into account the portion of incident quanta which was absorbed, quanta distribution in the light source spectrum, and difference in PL spectra between LGS and sodium salicylate. We calculated the integral PL as an area under the $I = f(h\nu)$ curve and plotted versus temperature in Fig. 12. For the F-center, the PL temperature dependence is well described in the Mott model with two recombination channels, one radiative and one nonradiative, from the relaxed excited state [21]. Here the temperature dependence of quantum efficiency η follows the expression

$$\eta(T) \approx \frac{1}{1 + \tau_R \nu_0 \, \exp\left(-\frac{\Delta E}{kT}\right)}, \qquad (5)$$

where τ_R is the radiative lifetime at low temperature, ΔE is the energy barrier to the nonradiative decay route, and ν_0 is a jump frequency. The proportional sign is used because other nonradiative decay channels must be available before the system reaches the relaxed excited state. The experimental points in Fig. 12b fit Eq. (5) with $\Delta E = 0.35$ eV and pre-exponential factor $\tau_R \nu_0 = 1.7 \times 10^4$ (solid line).

The pink STE emission at first rises ~3 times as temperature grows from 80 K then goes through the maximum at ~180 K and further decreases rather promptly with complete PL quenching at 400 K (Fig. 12a). The initial part of the PL temperature dependence at about 100 K may be described by an exponential factor $\sim \exp(-\Delta E_1/kT)$ with $\Delta E_1 \sim 0.02$ eV. Such buildup of PL may suggest an energy barrier ~0.02 eV to overcome at exciton self-trapping [20].

The broad bands that are observed in the PL spectra arise because the electron in the relaxation process interacts with the whole spectrum of normal modes of the defect lattice. The temperature dependence of the emission-band FWHM, $H(T)$, is described by the expression [21]

$$H^2(T) = H(0) \coth\left(\frac{h\bar{\omega}}{2kT}\right), \qquad (6)$$

where $H(0)$ is the FWHM at low temperature and $\bar{\omega}$ is the weighted average over the frequencies of all the defect-lattice modes that couple to the excited electronic state. The dots in Fig. 13a show the temperature dependence of the FWHM for PL 2.986 and 2.42 eV bands in coordinates arc $\coth(H^2(T)/H^2(80 \text{ K})) = f(1/T)$, whereas the same for PLE
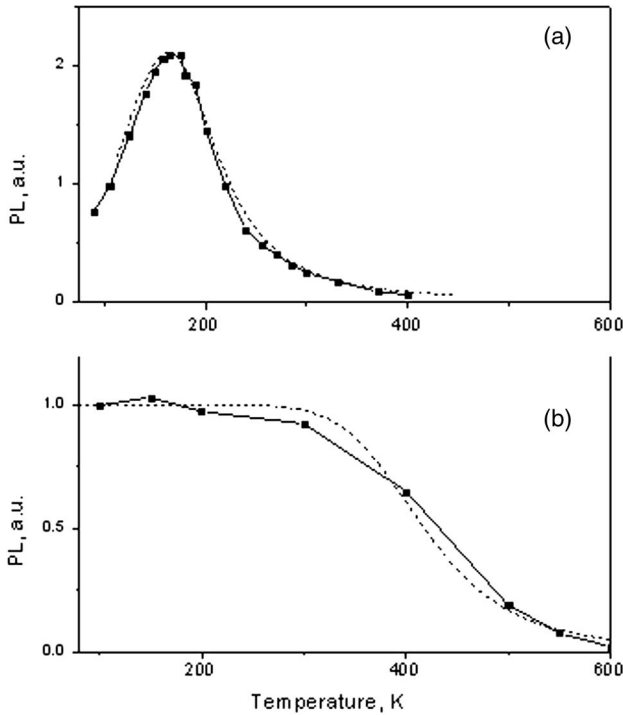

Fig. 12. Temperature dependence for integral PL emission in 1.9 eV (a) and 2.986 eV (b) bands in LGS at 4.0 eV and 3.4 eV excitations, respectively. Experimental data are shown as points, whereas dotted curves correspond to calculation according to Eq. (3) with parameters $\Delta E = 0.14$ eV, $\tau_R \nu_0 = 4 \times 10^3$ (a) and $\Delta E = 0.35$ eV, $\tau_R \nu_0 = 1.7 \times 10^4$ (b). In the case of (a), the initial stage is determined by the exponential rise with $\Delta E_1 \sim 0.02$ eV (activation barrier for exciton self-trapping).
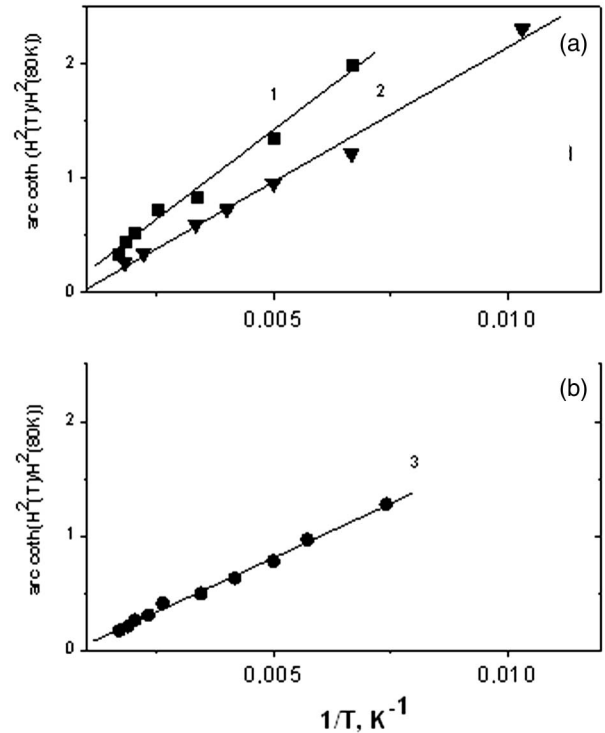

Fig. 13. Temperature dependence of the FWHM for 2.98 and 2.42 eV bands in PL spectra 1 and 2 and 3.38 eV band in PLE (Curve 3) in coordinates arc $\coth(H(T)/H(80 \text{ K}))$ versus $1/T$, in LGS, annealed in vacuum. The straight lines show the approximation according to Eq. (4) with the $h\bar{\omega}$ parameters: 50 meV (400 cm⁻¹), 39 meV (315 cm⁻¹), and 32 meV (260 cm⁻¹), respectively. At 80 K, the FWHM values are 0.22, 0.25, and 0.13 eV for Curves 1, 2, and 3, respectively.

is given in Fig. 13b. The later data are related only to the high-energy PLE Gaussian component in the inset of Fig. 10. As the FWHM does not change in the range of 80 to 150 K, we can take the value at 80 K as low-temperature $H(0)$. Experimental temperature dependencies are well approximated by straight lines in accord with Eq. (4). The obtained values of $h\bar{\omega}$ are 50 meV (400 cm^{-1}) and $h\omega = 39$ meV (315 cm^{-1}) for PL bands 2.98 and 2.42 eV, and for the PLE high-energy component at 3.38 eV, we obtained $h\bar{\omega} = 32$ meV (260 cm^{-1}) in LGS. These values are realistic as they are within the range of vibrations of perfect LGS lattice according to Raman spectroscopy data in Fig. 3. The range of phonon energies in LGS is 70 to 450 cm^{-1} or 8 to 55 meV. The vibrations responsible for temperature broadening of PL spectra are close to Li–S vibrations in a perfect LGS lattice.

The Huang–Rhys factor S, a parameter used to describe the strength of the linear electron–lattice interaction, is related to the second moment of the emission-band shape function [22]. The physical meaning of S is an average number of phonons participating in the absorption/PL process. A relative estimate for the Huang–Rhys factor can be obtained based on the semi-classical configuration coordinate diagram [23]. With the assumption of parabolic potential curves and equal ground- and excited-state effective vibronic frequencies, the low-temperature Stokes shift is given as $E_{abs} - E_{emi} = h\bar{\omega}(2S - 1)$; insertion of the experimental quantities yields S values 5 to 6.5. The magnitude of the Huang–Rhys factor is related to the probability of observing a zero-phonon line (ZPL) in absorption and emission. The ratio of the integrated intensities of ZPL to the broad band is expected to be e^{-S}. Failure to observe a ZPL near 3.1 eV in moderately high-resolution absorption ($\Delta\lambda \sim 0.05$ nm) and emission ($\Delta\lambda \sim 0.5$ nm) spectra taken near 80 K demonstrates $S > 5$, in agreement with the above estimates. The Huang–Rhys factor for F-center in LGS, therefore, lies intermediate between the strong coupling reported for MgO ($S = 35$) in [23] and the weak coupling reported for diamond ($S \sim 0.5$ to 1 with a well-pronounced ZPL) [24].
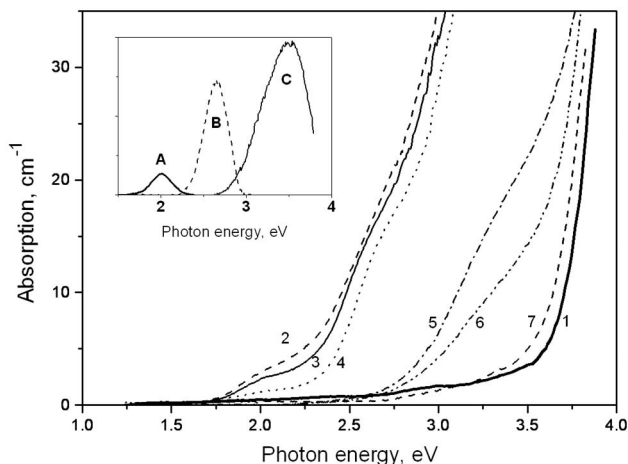

Fig. 14.   Absorption spectra of LGS single crystals before (Curve 1) and after (Curve 2) irradiation with 3.5 MeV electrons. Spectra 2–7 show absorption spectra after annealing of irradiated LGS during 5 min at 100, 200, 300, 320, and 350 K, respectively. Individual components in the absorption spectrum of irradiated LGS are given in the inset. All spectra were recorded at $T = 80$ K.
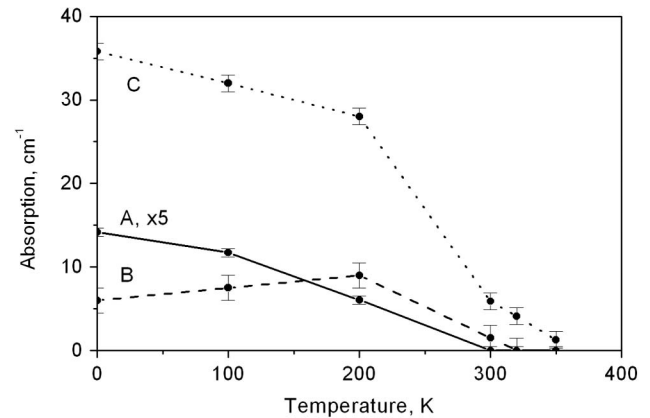

Fig. 15.   Temperature dependence of absorption in individual components at 2.0 eV (Band A), 2.65 eV (Band B), and 3.5 eV (Band C) at isochronic annealing. Absorption was measured in the band maximum for Bands A and B and in the low-energy wing (at $h\nu = 3.0$ eV) for Band C.

G. Absorption Induced by Ionizing Radiation

The alternative way to produce anion vacancy in inorganic solids is the ionizing irradiation with neutrons, protons, or fast electrons, and a large experience is accumulated when investigating alkali halide, oxide (particularly Al_2O_3 and MgO), fluoride, and other crystals [19]. In this work we irradiated LGS crystals with fast electrons of the 3.5 MeV energy to produce the F-centers. Figure 14 shows that the absorption spectra of LGS before and after electron irradiation as well as after annealing during 5 min at different temperatures in the range of 20 °C to 400 °C are given. One can see that strong absorption at $h\nu > 1.7$ eV appears after such irradiation. It weakens as crystal is warmed step by step and decreases completely near $T = 350$ °C. We separated three individual bands in the LGS spectrum: they are given in the inset in Fig. 14. A superposition of these bands produces the resulting absorption spectra of irradiated LGS. The maximums of these bands are located at 2.0, 2.65, and 3.4 eV. Here the latter is the most intense and is ~2 orders stronger than the 2.0 eV component. This intense band at 3.4 eV in irradiated LGS is similar to the absorption band 3.4 eV in LGS after annealing in vacuum, and corresponding defects are responsible for blue or violet PL. Thus, we produce the F-centers and some other point defects at irradiation. Temperature dependence for these three components is given in Fig. 15. We see that the intensity of two bands, at 3.4 and 2.0 eV, decreases steadily as annealing temperature grows, whereas the 2.65 eV component demonstrates a maximum near 200 °C. The inclination of annealing curves for 3.4 and 2.0 eV components already near room temperature implies that anion vacancies are moveable already room temperature and some defect transformations take place at about 200 °C. This fact agrees well with the above-mentioned transformation $V_{S1} \to V_{S2}$, which takes place at room temperature. The buildup of the 2.65 eV band near 200 °C during annealing is likely due to F-centers aggregation, and some complexes, probably F_2, appear.

4. CONCLUSIONS

Two PL systems with main bands at 2.74 and 2.98 eV in nonlinear LGS crystals were associated with two types of F-centers: sulfur vacancies V_{S1}, V_{S2}. They are responsible for absorption in the 3.4 eV band. These centers can be

produced at annealing in vacuum or at irradiation with fast electrons with 3.5 MeV energy, and they disappear after annealing in the presence of S-containing solids or after annealing if produced by irradiation. The V_{S1} centers appear the first at annealing, but afterward they transform into more stable centers V_{S2} when stored during several months at room temperature. For V_{S2}, PL decay is exponential with $\tau = 19$ μs and 218 ns at 80 and 300 K, respectively, with complete PL quenching at 650 K. Irradiation produces a set of radiation defects, including the F-centers, which transform into each other during annealing and annihilate completely at 670 K. The vacancy migration takes place even at room temperature: as a result, the initially produced V_{S1} centers transform into V_{S2} in several months at room temperature.

A broadband PL near 2 eV excited near the fundamental absorption band, with a large Stokes shift of 2 eV and nonexponential decay, quenched at 400 K, is associated with recombination of STEs. There is an energy barrier for exciton self-trapping ~0.02 eV.

The chemically stable LGS crystals with a slow temperature quenching of the F-center-related PL may be used as active media for tunable solid-state lasers and also as multifunctional material, taking into account its good nonlinear susceptibility as well as a light emitting elements in different optoelectronic devices. In addition, concentration and spatial distribution of the F-centers give valuable information about the degree of LGS deviation from stoichiometry, growth conditions, and radiation history as well about its optical quality.

ACKNOWLEDGMENTS

REFERENCES

1. V. G. Dmitriev, G. G. Guzadyan, and D. N. Nikogosyan, *Handbook of Nonlinear Optical Crystals* (Springer, 1999).
2. A. P. Yelisseyev, L. I. Isaenko, S. I. Lobanov, J.-J. Zondy, A. Douillet, I. Thenot, Ph. Kupecek, G. Minnerat, J. Mangin, S. Foussier, and S. Salaun, "New ternary sulfide for double application in laser scheme," in *OSA TOPS Advanced Solid State Lasers*, Vol. **34** of OSA Advanced Solid State Lasers, H. Injevan, U. Keller, and C. Marshall, eds. (Optical Society of America, 2000), pp. 561–568.
3. J.-J. Zondy, V. Petrov, A. Yelisseyev, L. Isaenko, and S. Lobanov, "Orthorhombic crystals of lithium thioindated and selenoindate for nonlinear optics in the mid-IR," in *Mid-Infrared Coherent Sources and Applications*, NATO Science for Peace and Security Series, B: Physics and Biophysics, M. Ebrahim-Zadeh and I. Sorokina, eds. (Springer, 2008), pp. 67–104.
4. V. Petrov, A. Yelisseyev, L. Isaenko, S. Lobanov, A. Titov, and J.-J. Zondy, "Second harmonic generation and optical parametric amplification in the mid-IR with orthorhombic biaxial crystals LiGaS$_2$ and LiGaSe$_2$," Appl. Phys. B **78**, 543–546 (2004).
5. L. Isaenko, I. Vasilyeva, A. Yelisseyev, S. Lobanov, V. Malakhov, L. Dovlidova, J.-J. Zondy, and I. Kavun, "Growth and characterization of LiInS$_2$ single crystals," J. Cryst. Growth **218**, 313–322 (2000).
6. J. Leal-Gonzalez, S. S. Melibary, and A. J. Smith, "Structure of lithium gallium sulfide, LiGaS$_2$," Acta Crystallogr. C **C46**, 2017–2019 (1990).
7. L. Isaenko, A. Yelisseyev, S. Lobanov, P. Krinitsin, V. Vedenyapin, and J. Smirnova, "Growth and properties of LiGaX$_2$ (X = S, Se, Te) single crystals for nonlinear application in the mid-IR," Cryst. Res. Technol. **38**, 379–387 (2003).
8. T. S. Moss, *Optical Properties of Semiconductors* (Butterworth, 1961).
9. R. Alison, J. Burns, and A. J. Tuzzolino, "Absolute fluorescent quantum efficiency of sodium salicylate," J. Opt. Soc. Am. **54**, 747–750 (1964).
10. S. Fossier, S. Salaun, O. Bidault, I. Thenot, J.-J. Zondy, W. Chen, F. Rotermund, V. Petrov, P. Petrov, J. Henningsen, A. Yelisseyev, L. Isaenko, S. Lobanov, O. Balachninaite, G. Slekys, and V. Sirutkaitis, "Optical, vibrational, thermal, damage and phase-matching properties of lithium thioindate," J. Opt. Soc. Am. B **21**, 1981–2007 (2004).
11. L. Bai, Z. S. Lin, Z. Z. Wang, and C. T. Chen, "Mechanisms of linear and nonlinear effects of chalcopyrites LiGaX$_2$ (X = S, Se and Te) crystals," J. Appl. Phys. **103**, 083111 (2008).
12. J. Aarik, H. Mandar, M. Kirm, and L. Pung, "Optical characterization of HfO$_2$ thin films grown by atomic layer deposition," Thin Solid Films **466**, 41–47 (2004).
13. G. C. Catella and D. Burlage, "Crystal growth and optical properties of AgGaS$_2$ and AgGaSe$_2$," MRS Bull. **23**, 28–36 (1998).
14. V. Petrov, J.-J. Zondy, O. Bidault, L. Isaenko, V. Vedenyapin, A. Yelisseyev, W. Chen, A. Tyazhev, S. Lobanov, G. Marchev, and D. Kolker, "Optical, thermal, electric, damage and phase-matching properties of lithium selenoindate," J. Opt. Soc. Am. B **27**, 1902–1927 (2010).
15. R.-M. Nigge, F. P. Baumgartner, and E. Bucher, "CVT growth of AgGaSe$_2$ single crystals: electrical and photoluminescence properties," Sol. Energy Mater. Sol. Cells **43**, 335–343 (1996).
16. L. Bonch-Bruevich and V. B. Glasko, "To theory of dislocations-related electronic transitions," Sov. Phys. Solid State **3**, 36–52 (1961).
17. V. F. Kokorina, *Glasses for Infrared Optics* (CRC Press, 1996).
18. HSC chemistry software, http://www.chemistry-software.com.
19. W. B. Fowler, ed., *Physics of Color Centers* (Academic, 1968), Chaps. 2 and 4.
20. K. S. Song and R. T. Williams, *Self-Trapped Excitons* (Springer, 1993).
21. B. Henderson and G. F. Imbusch, *Optical Spectroscopy of Inorganic Solids* (Clarendon, 1989).
22. W. C. Ward and E. B. Hensleym, "Additive coloration of calcium oxide," Phys. Rev. **175**, 1230–1232 (1968).
23. B. D. Evans and J. C. Kemp, "Vibrational aspects of the CaO and MgO F bands," Phys. Rev. B **B2**, 4179–4189 (1970).
24. A. M. Zaitsev, *Optical Properties of Diamond: Data Handbook* (Springer, 2001).